GRK5 promotes F-actin bundling and targets bundles to membrane structures to control neuronal morphogenesis

Yuejun Chen,[1,2] Feifei Wang,[1,2] Hui Long,[1,2] Ying Chen,[1,2] Ziyan Wu,[1,2] and Lan Ma[1,2]

[1]The State Key Laboratory of Medical Neurobiology and [2]Pharmacology Research Center, Shanghai Medical College and Institutes of Brain Science, Fudan University, Shanghai 200032, China

Neuronal morphogenesis requires extensive membrane remodeling and cytoskeleton dynamics. In this paper, we show that GRK5, a G protein–coupled receptor kinase, is critically involved in neurite outgrowth, dendrite branching, and spine morphogenesis through promotion of filopodial protrusion. Interestingly, GRK5 is not acting as a kinase but rather provides a key link between the plasma membrane and the actin cytoskeleton. GRK5 promoted filamentous actin (F-actin) bundling at the membranes of dynamic neuronal structures by interacting with both F-actin and phosphatidylinositol-4,5-bisphosphate. Moreover, separate domains of GRK5 mediated the coupling of actin cytoskeleton dynamics and membrane remodeling and were required for its effects on neuronal morphogenesis. Accordingly, GRK5 knockout mice exhibited immature spine morphology and deficient learning and memory. Our findings identify GRK5 as a critical mediator of dendritic development and suggest that coordinated actin cytoskeleton and membrane remodeling mediated by bifunctional actin-bundling and membrane-targeting molecules, such as GRK5, is crucial for proper neuronal morphogenesis and the establishment of functional neuronal circuitry.

Introduction

During development, neuronal cells undergo dramatic changes in morphology, which are critical for the establishment of neural circuitry and generation of neuronal plasticity (Luo, 2002). Altered neuronal morphology is associated with neural developmental disorders that affect human cognition, such as autism spectrum disorders, mental retardation, and fragile X and Down's syndromes (Fiala et al., 2002; Newey et al., 2005; Dierssen and Ramakers, 2006; Penzes, 2007). Neuronal morphogenesis, including neurite initiation, outgrowth, branching, and spine formation, requires the cytoskeleton and membrane to undergo dynamic changes. By exerting mechanical forces that alter the shape of the plasma membrane, the actin cytoskeleton remodeling plays a key role in morphogenesis of neurons and other eukaryotic cells (da Silva and Dotti, 2002; Pollard and Borisy, 2003; Suetsugu and Takenawa, 2003; Newey et al., 2005).

Filopodia are critically involved in neurite initiation (Dent et al., 2007; Kwiatkowski et al., 2007), growth cone dynamics (Gallo and Letourneau, 2004; Burnette et al., 2007), and dendrite branching (Gallo and Letourneau, 1998; Dent et al., 2004) and are considered as precursors for presynaptic terminals and postsynaptic spines (Dailey and Smith, 1996; Ahmari and Smith, 2002). Studies indicate that the formation of filopodial protrusions primarily depends on proteins regulating actin polymerization at the barbed end of actin filaments, bundling F-actin, and deforming the membrane (Gupton and Gertler, 2007; Guerrier et al., 2009). A functional relationship between filopodial protrusion and neuronal morphogenesis and the critical involvement of both membrane components and cytoskeleton in the processes have been proposed (Scita et al., 2008; Carlson and Soderling, 2009; Yang et al., 2009).

Y. Chen, F. Wang, H. Long, and Y. Chen contributed equally to this paper.

Correspondence to Lan Ma: lanma@shmu.edu.cn

Abbreviations used in this paper: ANOVA, analysis of variance; BK, bradykinin; DIV, day in vitro; EmGFP, Emerald GFP; G-actin, globular actin; GPCR, G protein–coupled receptor; GRK, GPCR kinase; KO, knockout; miRNA, microRNA; PAO, phenylarsine oxide; PC, phosphatidylcholine; PI(4,5)P2, phosphatidylinositol-4,5-bisphosphate; TDBTN, total dendritic branch tip number; WT, wild type.

The Rockefeller University Press $30.00
J. Cell Biol. Vol. 194 No. 6 905–920
www.jcb.org/cgi/doi/10.1083/jcb.201104114

However, how neurons spatiotemporally coordinate actin dynamics and membrane remodeling during morphogenesis remains to be elucidated.

G protein–coupled receptor (GPCR) kinases (GRKs) are known as a family of serine/threonine kinases that desensitize GPCR signaling by phosphorylating agonist-occupied receptors. GRK-catalyzed receptor phosphorylation leads to the recruitment of arrestins to the cell membrane and the internalization of GPCRs and, thus, regulates cellular responses to extracellular signals (Kohout and Lefkowitz, 2003; Lefkowitz, 2007). Extensive studies have focused on GRK-mediated phosphorylation and regulation of various GPCRs in the past two decades. The important roles of various subtypes of GRKs (GRK1–7) in regulating physiological functions of specific GPCRs have been demonstrated in vivo (Métayé et al., 2005; Premont and Gainetdinov, 2007). However, these physiological functions of GRKs have mainly been ascribed to their role of phosphorylating and desensitizing GPCRs.

Emerging evidence indicates that GRKs are also capable of interacting with nonreceptor proteins noncatalytically. It has been shown that GRK2 interacts with Gαq to regulate GPCR signaling (Carman et al., 1999), and binding of GRK5 with IκBα inhibits NF-κB–mediated transcription (Sorriento et al., 2008). Our recent study demonstrated that kinase activity–independent regulation of the cyclin pathway by GRK2 is essential for zebrafish early development (Jiang et al., 2009). Freeman et al. (1998) reported that actin can bind to GRK5 and inhibit its kinase activity in vitro. Accumulating data imply that GRKs may exert multiple functions in vivo via mechanisms, including those independent of their catalytic function toward receptor substrates.

The current study reveals a previously unrecognized role for GRK5 in the regulation of neuronal development. We demonstrate that GRK5 functions as an actin-bundling scaffold as well as a linkage between bundled actin filament and phosphatidylinositol-4,5-bisphosphate (PI(4,5)P2)–rich membrane during neuronal morphogenesis and thus promotes neuronal filopodial formation, neurite outgrowth, dendrite branching, and spine maturation.

Results

GRK5 regulates dendritic development

To explore the potential role of GRK5 in neuronal development, the expression of GRK5 in hippocampus and cortex of developing rat brain was examined. As shown in Fig. S1 A, peak expression of GRK5 was detected between postnatal day 7 and 21 (P7–P21), a period of intense dendritic development. The effect of GRK5 on dendritic development was examined in primary neuron cultures (Fig. 1). Overexpression of GRK5 in hippocampal neurons at 5 d in vitro (DIV5) significantly increased dendrite length and total dendritic branch tip number (TDBTN); similarly, overexpression of K215R, the kinase-dead mutant of GRK5, induced a comparable effect on neuronal morphogenesis (Fig. 1 A). Stage 2 neurons overexpressing GRK5 or K215R also developed longer neurites with more branches (Fig. S1 B). Conversely, knockdown of endogenous GRK5 in cultured DIV5 neurons by GRK5 RNAi (Fig. S1 C) resulted in less complex dendritic structure, which can be rescued by cotransfection of bovine GRK5 or K215R (Fig. 1 B). In mature neurons, overexpression of GRK5 or K215R significantly increased the density of dendritic protrusion and dendritic spines and the proportion of spines in total protrusions (Fig. 1 C). Down-regulation of endogenous GRK5 in hippocampal neurons by GRK5 RNAi resulted in a decreased density of dendritic protrusions and spines, reduced percentage of spines (Fig. 1 D), and longer spines with smaller heads (Fig. S1 D). Furthermore, overexpression of GRK5 and K215R caused a significant increase of PSD-95–positive spines (Fig. S1 E), whereas GRK5 RNAi decreased the number of PSD-95–positive spines, indicating that GRK5 promotes the maturation of dendritic spines (Fig. S1 F).

The effect of GRK5 on neurite initiation was observed in Neuro-2a cells. Similar to nontransfected cells, most of Neuro-2a cells transfected with GFP alone were round, and only 8% of them had short, neuritelike, nonbranched extensions. Overexpression of GRK5 or K215R led to the production of long, branched, neuritelike processes, accompanied by many filopodia (Fig. S1, G and H). Collectively, these results indicate that GRK5 is critically involved in dendritic development, and the morphological effect of GRK5 does not depend on its catalytic activity.

GRK5 interacts with F-actin and promotes filopodia formation and dynamics

To investigate the mechanism through which GRK5 regulates dendritic development, the subcellular distribution of GRK5 was examined in living Neuro-2a cells. GRK5 overexpression induced growth cone–like structures in Neuro-2a cells, and GRK5-GFP fluorescence accumulated in these structures, exhibiting restricted distribution, and extensively colocalized with F-actin but not tubulin (Fig. S2, A and B). Colocalization of GRK5 with F-actin was also observed in membrane ruffles (Fig. S2 B) and at the roots of neurite branches as well as filopodia (Fig. S2 C). Real-time observations revealed that GRK5 and actin colocalized at the leading edge of growing neurites (Fig. S2 D). In cultured neurons, GRK5 fluorescence was accumulated and colocalized with F-actin in filopodia of growth cones and dendrite shafts (Fig. 2, A and B). In mature neurons, GRK5 distribution was enriched and colocalized with F-actin in the phalloidin-positive puncta in dendritic spines (Fig. 2 C). To further confirm subcellular distribution of endogenous GRK5 in cells, cultured neurons were stained with polyclonal antibodies against GRK5. Consistently, endogenous GRK5 was observed at the filopodia of growth cones and was colocalized with F-actin in DIV1 neurons (Fig. 2 D). In mature neurons, endogenous GRK5 was enriched in the dendritic spines and colocalized with F-actin (Fig. 2 E). The specificity of the GRK5 antibody was confirmed by a GRK5 RNAi experiment. Knockdown of GRK5 decreased the antibody staining (Fig. S2 E). Colocalization of GRK5 with F-actin was also observed in nonneuronal cells. For example, GRK5 was colocalized extensively with filopodia-like actin filaments but not with stress fibers in HeLa cells (Fig. S3 C).

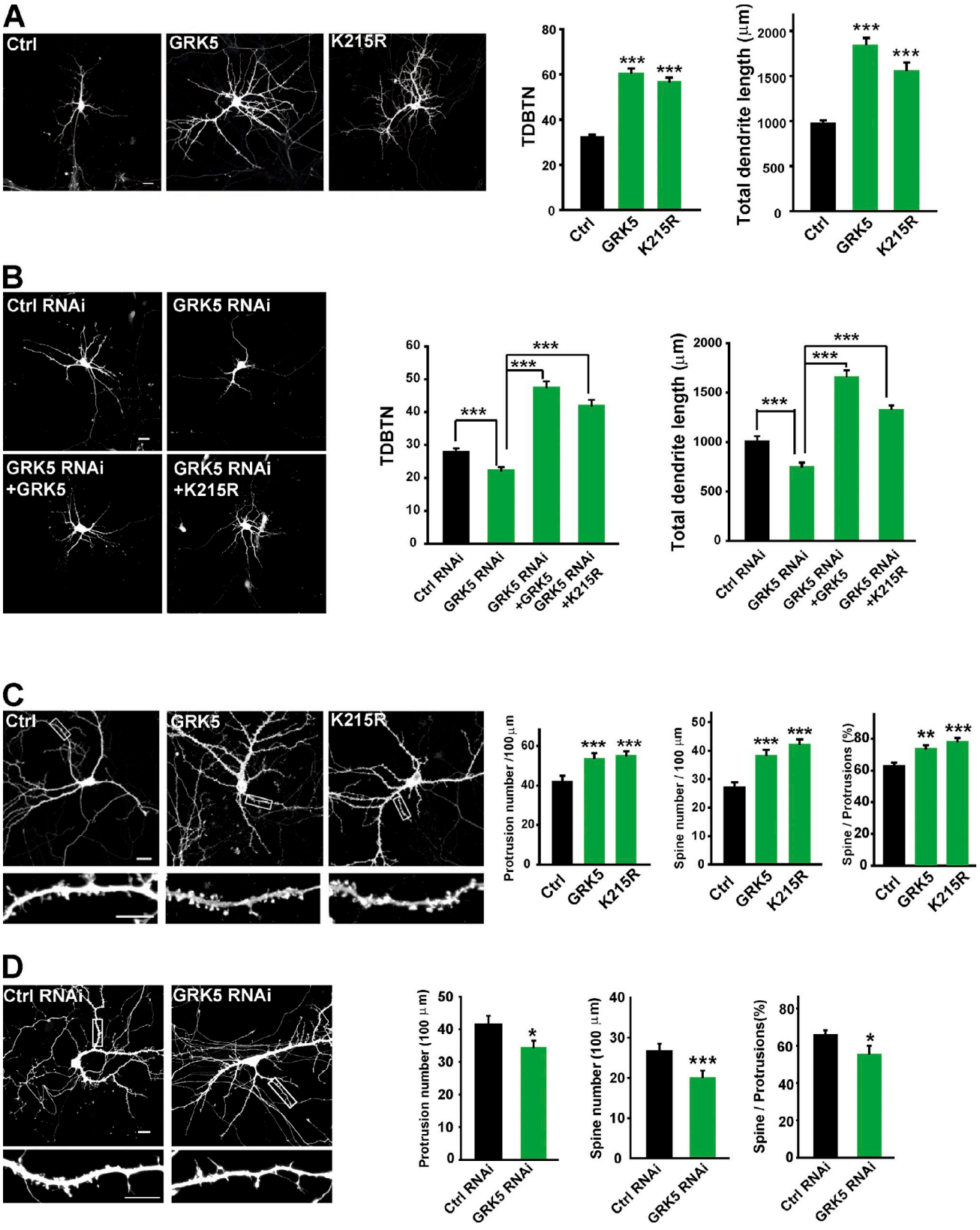

Figure 1. **GRK5 regulates dendritic development.** (A and B) Hippocampal neuron cultures transfected at DIV5 were observed at DIV8. Total dendritic branch tip numbers (TDBTN) and total dendrite length of transfected neurons were measured. For each group, 40–60 (A) or 30–40 (B) neurons from three independent cultures were analyzed. One-way ANOVA followed by Tukey–Kramer posthoc test. (C and D) Hippocampal neurons were transfected at DIV9 and observed at DIV17. Boxed regions are enlarged below each image. For each group, 30–40 dendrites of 8–10 neurons from three independent cultures were analyzed. Protrusion and spine number were measured. (C) GFP was cotransfected with GRK5 variants to visualize dendritic spines (one-way ANOVA followed by Tukey–Kramer posthoc test). (D) Neuron cultures transfected with control or GRK5 RNAi constructs (Student's *t* test). Bars, 10 μm. Error bars indicate SEM. *, $P < 0.03$; **, $P < 0.01$; ***, $P < 0.001$. Ctrl, control.

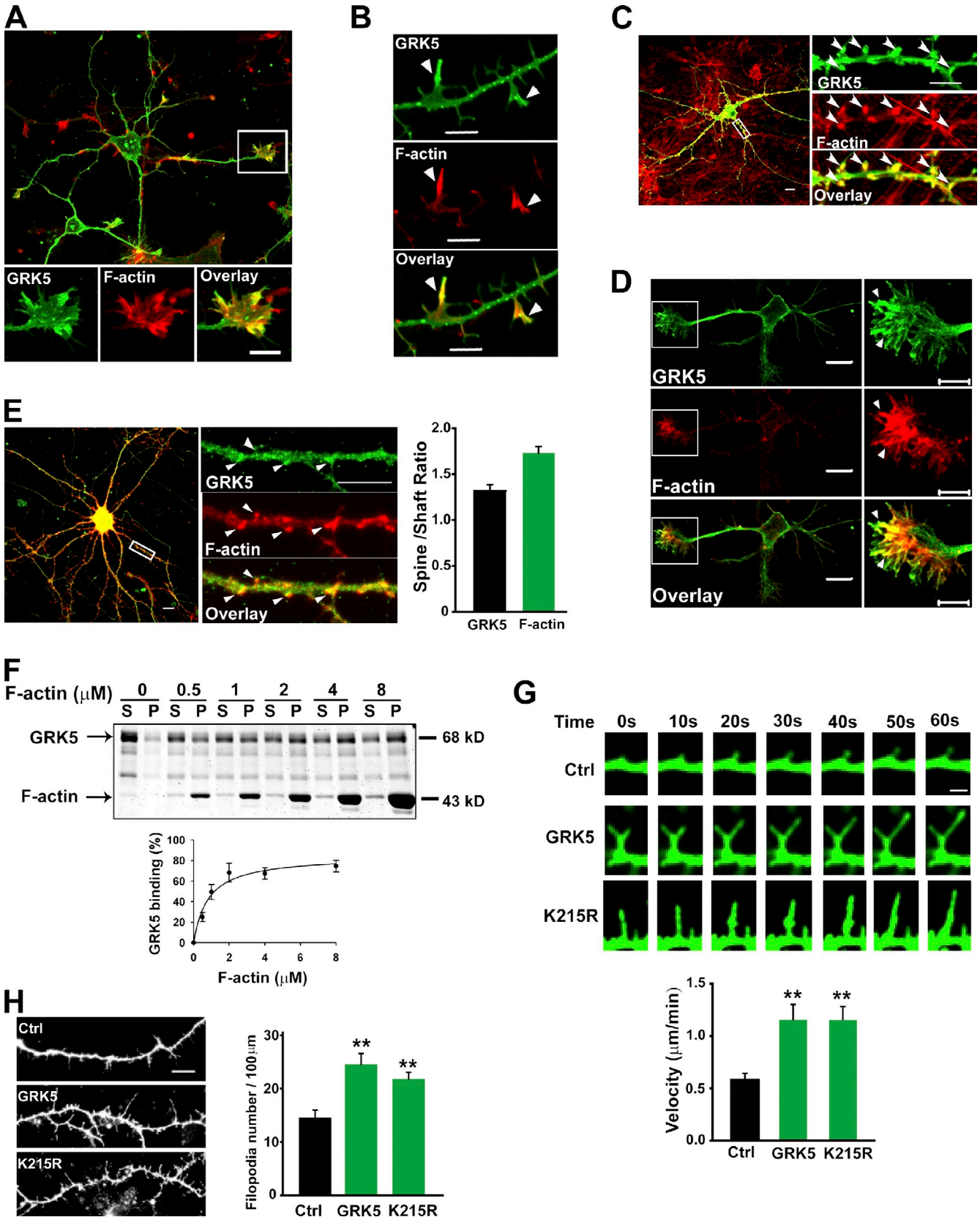

Figure 2. **GRK5 interacts with F-actin and promotes filopodia formation and dynamics.** (A–E) Colocalization of GRK5 with F-actin at sites of actin high dynamic structures. (A–C) Neurons were transfected with HA-tagged GRK5 and stained with HA antibody and Alexa Fluor 546 phalloidin. (A and B) Neurons transfected after dissection and stained at DIV2. (C) Neurons transfected at DIV9 and stained at DIV17. (B and C) Arrowheads indicate the colocalization of GRK5 with F-actin. (D and E) Neurons were stained at DIV1 (D) or at DIV14 (E) with GRK5 antibody (G-2) and Alexa Fluor 546 phalloidin. Arrowheads indicate the colocalization of GRK5 with F-actin in filopodia of growth cone (D) and dendritic spines (E). (E) The ratio of fluorescent intensity for GRK5 and

The F-actin–binding capacity of GRK5 was examined in a high-speed cosedimentation assay. Consistent with the previous study that actin can bind GRK5 and inhibit its kinase activity in vitro (Freeman et al., 1998), purified GRK5 bound to F-actin in a concentration-dependent and saturable manner (K_d, 0.809 ± 0.245 μM; Fig. 2 F). The interaction of GRK5 and F-actin could occur at both physiological and lower salt concentrations, whereas reduced association was detected under a high-salt condition (Fig. S2 F). The data that GRK5 regulates neurite initiation and dendrite branching, processes require filopodia protrusion, and GRK5 has a specialized localization in filopodia suggest the possible involvement of GRK5 in the induction of filopodial protrusion.

The effects of GRK5 on filopodial protrusion and dynamics were examined by time-lapse imaging in cultured hippocampal neurons. Stable filopodia, which did not change in length, and dynamic filopodia, which extended and retracted frequently during a 10-min recording period, were quantified in GFP-transfected neurons (Fig. 2 G). Of the filopodia examined, 31% (42/134) were dynamic, whereas in neurons transfected with GRK5 or K215R, the population of dynamic filopodia increased to 61–63% (123/195 for GRK5 and 109/178 for K215R). Meanwhile, transfection of GRK5 or K215R induced a significant increase in the velocity of filopodial movement (Fig. 2 G) as well as the number of filopodia (Fig. 2 H).

GRK5 rearranges F-actin into bundles, and this requires its C-terminal basic residues essential for F-actin binding

Filopodia are membrane protrusions formed with parallel bundles of actin filaments. The formation of filopodia is thought to be primarily dependent on proteins regulating actin polymerization at the barbed end of actin filaments, bundling F-actin, or deforming the membrane (Gupton and Gertler, 2007; Guerrier et al., 2009). The interaction of GRK5 with F-actin and the localization of GRK5 at sites of actin-rich, highly active structures, such as filopodia, indicate that GRK5 may play a role in actin dynamics. The results of actin polymerization experiments indicated that GRK5 had no detectable actin nucleation activity by itself (Fig. S3 A), and it did not alter the nucleation activity of the Arp2/3 complex (not depicted) or VCA (verprolin homology, cofilin, and acidic domain contained in the N-WASP C-terminal fragment)-induced Arp2/3 nucleation activity (Fig. S3 B). However, the architecture of actin filament polymerized was clearly changed in the presence of GRK5. As shown in Fig. 3 A, in the absence of GRK5, actin filaments showed a diffused network, not bundles. The presence of GRK5 resulted in prominent actin bundles, and a single bundle, as well as extensive networks of bundles, was observed. Both the quantity and size of bundles increased with GRK5 concentration. Similar results were observed when GRK5 was added after F-actin had already formed (unpublished data). The effect of GRK5 on actin bundling was also assessed in an alternative, low-speed sedimentation assay. Incubation of F-actin with increasing concentrations of purified GRK5 resulted in a concentration-dependent increase of the fraction of F-actin in the pellet, demonstrating increased formation of F-actin bundles (Fig. 3 B). These results suggest that GRK5 may act as an actin-bundling scaffold.

To identify the F-actin binding domain in GRK5, a series of GRK5 mutants were constructed (Fig. 3 C). Fluorescence cell imaging analysis of the colocalization of F-actin with various GRK5 truncation mutants indicated that the C-terminal domain of GRK5 is necessary and sufficient for its interaction with F-actin, and the basic amino acid–enriched sequence within the C terminus is critical (Fig. 3 C and Fig. S3 D). Direct binding experiments demonstrated that a GRK5 mutant carrying alanine substitutions of these basic amino acids (C-PBA) failed to bind to F-actin, whereas K215R bound to F-actin to an extent comparable with wild-type (WT) GRK5 (Fig. 3 D). Consistent with actin-binding data, both visualization and low-speed sedimentation F-actin–bundling experiments demonstrated that K215R, but not the F-actin binding–deficient GRK5 mutant C-PBA, is capable of inducing actin bundle formation (Fig. 3, E and F). These results demonstrate that the binding of the GRK5 C terminus with F-actin is essential for its actin-bundling activity.

Ca^{2+}/calmodulin inhibits the F-actin–bundling activity of GRK5

The C-terminal stretch of basic amino acids required for F-actin binding and bundling overlaps with the calmodulin binding site previously localized to residues 552–561 of GRK5 (Pronin et al., 1997; Levay et al., 1998). Thus, experiments were performed to determine whether competition of calmodulin with F-actin for binding to the GRK5 C terminus regulates actin bundle formation. Indeed, Ca^{2+}/calmodulin concentration dependently inhibited GRK5- or K215R-mediated actin bundle formation (Fig. 3 G), whereas $CaCl_2$ itself had no effect (not depicted). The inhibitory effect of Ca^{2+}/calmodulin was also observed in a low-speed cosedimentation assay (Fig. 3 H). These data support the premise that the C terminus of GRK5 binds with F-actin and facilitates bundling of F-actin. Our coimmunoprecipitation experiments demonstrated the self-association of GRK5 in cells (Fig. S3 E), and we thus postulate that GRK5 may form dimers or oligomers by self-association to cross-link F-actin into bundles.

F-actin in spines versus shafts was plotted. (F) High-speed sedimentation F-actin–binding assays. 1 μM purified GRK5 was incubated with F-actin for 30 min. Samples were centrifuged at 350,000 *g* for 30 min, and the supernatant (S) and the resuspended pellet (P) were analyzed by SDS-PAGE and Coomassie blue staining. The percentages of GRK5 bound to F-actin were calculated as the percentage recovered in the pellet subtracted by that recovered in the pellet without F-actin of five independent experiments. (G) GRK5 promotes the dynamics of filopodia. Time-lapse series of a neuron 2 d after transfection with the indicated constructs. Images shown are high-magnification images of a filopodial elongating from the shaft of the dendrite. The filopodial elongation/withdrawal velocities were measured. **, $P < 0.003$ (one-way ANOVA followed by Tukey–Kramer posthoc test). (H) GRK5 promotes the formation of filopodia-like protrusions. Shown are selected neuritic regions from DIV2 neurons transfected with the indicated constructs. GFP was cotransfected with GRK5 variants to visualize dendrite and filopodia. Protrusion densities were measured. **, $P < 0.01$ (one-way ANOVA followed by Tukey–Kramer posthoc test). Error bars indicate SEM. Boxed regions in images indicate enlarged areas. Ctrl, control. Bars: (A and B) 5 μm; (C–E and H) 10 μm; (G) 1 μm.

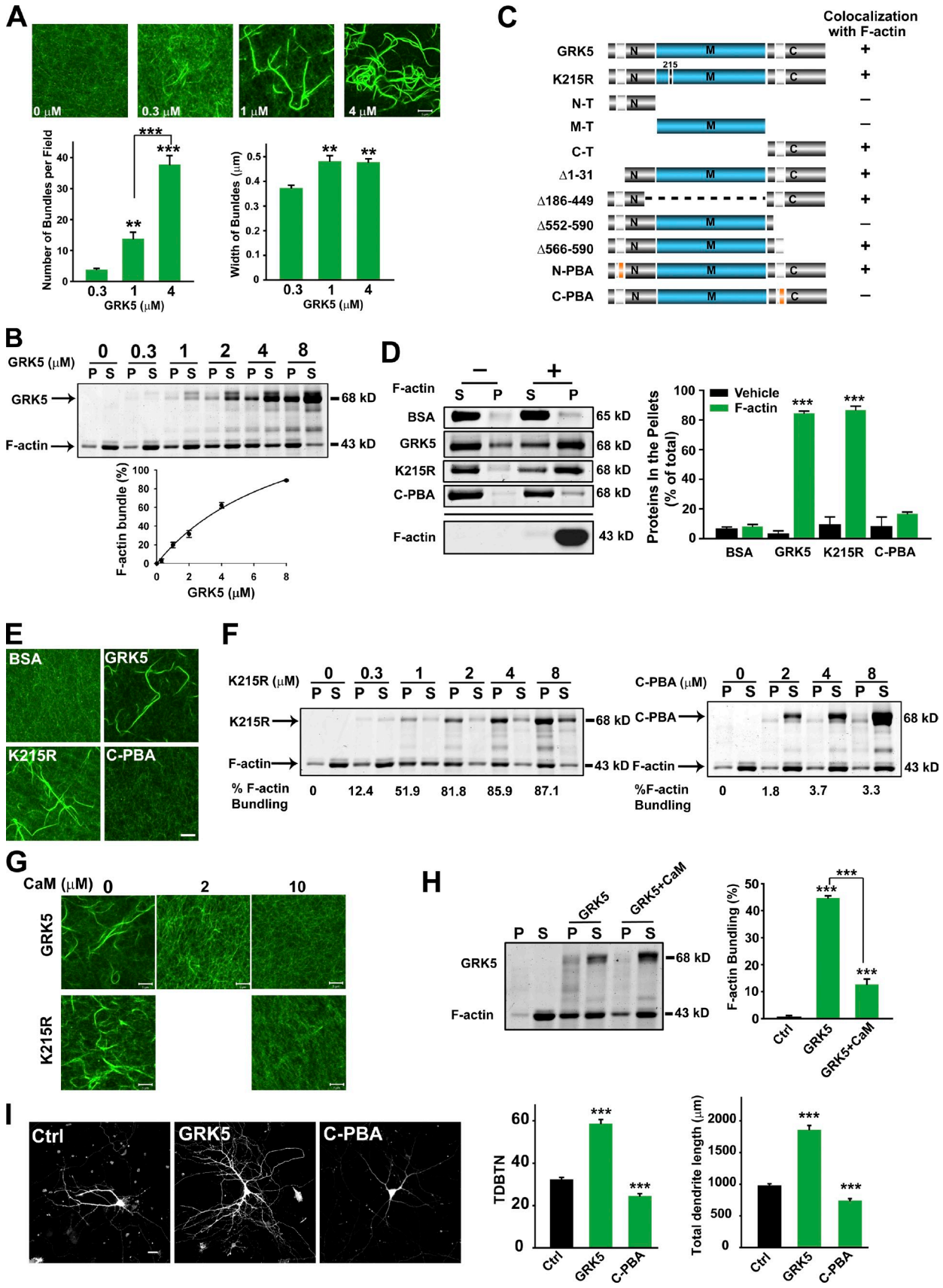

Figure 3. **GRK5 rearranges F-actin into bundles, and this requires its C-terminal basic residues essential for F-actin binding.** (A, E, and G) Visualization of F-actin bundles by confocal microscopy. Alexa Fluor 488–labeled G-actin was polymerized in the presence of the indicated concentration of purified GRK5 (A), 1 μM BSA or purified GRK5 variants, or 2 μM GRK5 variants in the presence or absence of indicated concentrations of Ca^{2+}/calmodulin. The number of F-actin bundles in five randomly selected images from three independent experiments was analyzed. The thickest region of F-actin bundles was

The actin-binding/bundling activity of GRK5 is critical for its effect on filopodial formation and dendritic development

We next examined whether the effect of GRK5 on filopodial protrusion and dendritic development is dependent on actin-binding/bundling activity. Overexpression of GRK5, K215R, or Δ566–590 (a mutant lacking the C-terminal 25 residues but retaining the basic amino acid stretch required for F-actin binding/bundling) in Neuro-2a cells substantially increased the number of neurite-bearing cells and the length of neurites. However, disrupting the basic amino acid cluster required for F-actin binding/bundling by C-terminal deletion (Δ552–590) or substitution (C-PBA) greatly impaired GRK5-induced neurite initiation (Fig. S4 A).

The importance of the F-actin–binding/bundling function of GRK5 in neuronal morphogenesis was also demonstrated in cultured neurons. In contrast to WT GRK5, overexpression of C-PBA failed to promote neurite outgrowth or elongation in stage 2 neurons (Fig. S4 B). Moreover, overexpression of C-PBA decreased dendrite length and TDBTN at DIV5 neurons (Fig. 3 I). These data confirm that the observed effects of GRK5 on filopodial protrusion and dendritic development are crucially dependent on its F-actin–binding/bundling property.

The effects of GRK5 on filopodial dynamics and dendritic development depend on its PI(4,5)P2-binding capability

We next explored how the effect of GRK5 on neuronal morphogenesis is regulated. PI(4,5)P2 plays a key role in transmitting signals from the plasma membrane to the actin cytoskeleton by direct interaction and activation of several actin-binding proteins (Doherty and McMahon, 2008). GRK5 has been shown to interact directly with PI(4,5)P2 through the basic residue stretch in its N terminus, and PI(4,5)P2-mediated membrane association of GRK5 is required for targeting GRK5 to receptor substrates (Pitcher et al., 1996). The potential involvement of PI(4,5)P2 in GRK5-promoted filopodia dynamics and dendritic development was investigated. We manipulated the PI(4,5)P2 level by activating bradykinin (BK) receptors, which could activate Gq and stimulate PLC-mediated PI(4,5)P2 breakdown. Phenylarsine oxide (PAO), an inhibitor of phosphatidylinositol 4 kinase, was applied to block recovery of PI(4,5)P2 after BK receptor activation (van Rheenen and Jalink, 2002). As shown in Fig. 4 A, the increase of TDBTN and dendrite length in hippocampal neurons induced by overexpression of GRK5 was blocked by cotreatment of BK and PAO. The effect of down-regulation of PI(4,5)P2 on filopodial dynamics was observed in real time. After BK and PAO cotreatment, the velocity of filopodial movement was significantly reduced in neurons expressing GRK5 (Fig. 4 B). Consistent with the inhibitory effect of Ca^{2+}/calmodulin on the F-actin–bundling activity of GRK5, the filopodial motility in neurons overexpressing GRK5 was inhibited by ionomycin, a calcium ionophore (Fig. 4 B). BK could also increase cytosolic 3,4,5-bisphosphate, which may induce Ca^{2+}-dependent signaling. Thus, we used a more specific method to deplete PI(4,5)P2: rapamycin-induced membrane translocation of Inp54p, a yeast inositol polyphosphate 5-phosphatase that specifically cleaves the phosphate at position 5 of PI(4,5)P2 (Suh et al., 2006). Neurons were transfected with GRK5, Lyn11-FRB (Lyn), and CFP-FKBP-Inp54p (Inp) or the phosphatase-dead mutant of Inp54p (D281A). Rapamycin treatment resulted in reduced motility of filopodia in neurons expressing GRK5, Lyn, and Inp, whereas it had no effect on filopodial dynamics in cells expressing GRK5, Lyn, and D281A (Fig. 4 B). These results suggest that GRK5-mediated filopodial protrusion and dendritic development is regulated by membrane PI(4,5)P2.

We then mutated the N-terminal basic amino acid cluster, which mediates GRK5's interaction with PI(4,5)P2 (Pitcher et al., 1996). Overexpression of the N-terminal mutated GRK5 (N-PBA) failed to increase the motility and the number of filopodia as GRK5 and K215R did (Fig. 4 C and Fig. S4 C). Overexpression of C-PBA also failed to promote the motility of filopodia, and it decreased the number of filopodia (Fig. 4 C and Fig. S4 C). The TDBTN and total dendrite length in neurons transfected with N-PBA were also significantly lower than those transfected with the WT construct (Fig. 4 D), and transfection of neither N-PBA nor C-PBA could rescue the phenotypes of caused by GRK5 RNAi (Fig. S4 D). Consistent results on neurite morphology were observed in stage 2 neurons (Fig. S4 B). However, N-PBA could bind and bundle actin filaments as efficiently as WT GRK5 (Fig. S4, E and F), indicating that the actin bundle property of GRK5 is not sufficient for promoting filopodial protrusion and dendritic development, and direct binding of GRK5 with PI(4,5)P2 is also required. It should be noted that N-PBA expression in neurons also leads to a slight, but significant, increase in TDBTN and total dendrite length when compared with control neurons (Fig. 4 D and Fig. S4 C). We postulate that this may be attributed to the C-terminal domain–mediated actin-bundling activity of N-PBA.

As shown in Fig. S4 G, disruption of the kinase activity or the PI(4,5)P2-binding property of GRK5 did not affect its colocalization with F-actin and its predominant spine distribution

calculated as the width of F-actin bundles. 16–49 F-actin bundle filaments from each were analyzed. One-way ANOVA followed by Tukey–Kramer posthoc test. Bars, 5 µm. (B, F, and H) Low-speed sedimentation F-actin–bundling assay. Polymerized G-actin was incubated in the presence of an increasing concentration of purified GRK5 or 2 µM GRK5 variants in the presence or absence of 10 µM Ca^{2+}/calmodulin. After centrifugation at 10,000 *g*, the pellet (P) and the supernatant (S) were analyzed by SDS-PAGE and Coomassie blue staining. The percentage of F-actin present in the bundles was calculated as the percentage recovered in the pellet subtracted by that recovered in the pellet without GRK5. One-way ANOVA followed by Tukey–Kramer posthoc test. (C) Schematic presentation of GRK5 constructs and their colocalization with F-actin. N, M, and C refer to the N-terminal, middle, and C-terminal domains. White boxes refer to the regions containing the polybasic amino acid sequences in the N and C termini. Orange in white boxes indicates polybasic amino acid sequences with alanine substitutions (K22A, R23A, K24A, K26A, K28A, and K29A in N terminus and K547A, K548A, R553A, K556A, and R557A in C terminus). (D) High-speed sedimentation F-actin–binding assay. The percentages of proteins bound to F-actin were calculated as the percentage recovered in the pellet of three independent experiments. Student's *t* test. (I) Hippocampal primary neuron cultures were transfected with GFP or GFP with GRK5 or C-PBA at DIV5 and were observed at DIV8. Values of 40–60 neurons from three independent cultures were analyzed. One-way ANOVA followed by Tukey–Kramer posthoc test. Bar, 10 µm. Error bars indicate SEM. **, $P < 0.01$; ***, $P < 0.001$. Ctrl, control.

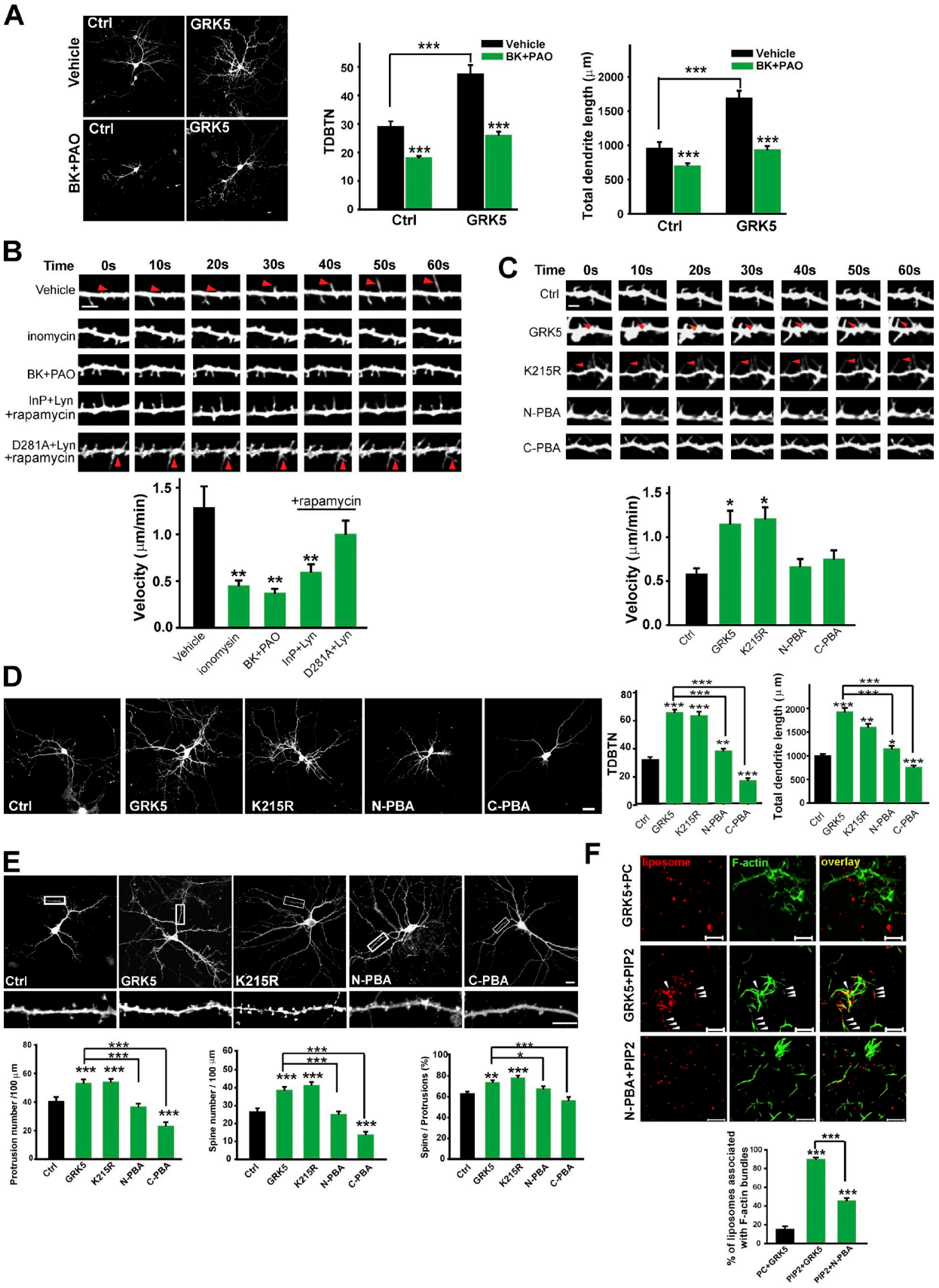

Figure 4. **The effects of GRK5 on filopodial dynamics and dendritic development depend on its PI(4,5)P2-binding capability.** (A) Hippocampal neuron cultures transfected with GFP or GFP and GRK5 at DIV5 were treated at DIV8 with 1 μm PAO and 100 nM BK (BK+PAO) for 8 h. Values of 20–30 neurons from three independent cultures were analyzed. One-way ANOVA followed by Tukey–Kramer posthoc test. (B and C) Time-lapse series of filopodial dynamics of hippocampal primary neurons at DIV2. Images were taken every 10 s, and filopodial elongation/withdrawal rates were measured. (B) Neurons

in mature neurons (Fig. S4 G). In contrast, C-PBA, the F-actin binding–deficient mutant of GRK5, was poorly colocalized with F-actin in the dendritic spines and showed a significantly decreased ratio of spine/shaft distribution (Fig. S4 G). Furthermore, overexpression of GRK5 or K215R, but not N-PBA or C-PBA, significantly increased dendritic protrusions, dendritic spines, and the percentage of spines in total protrusions in mature neurons (Fig. 4 E). On the contrary, overexpression of C-PBA resulted in a decrease in total number of dendritic protrusions and both the number and the percentage of dendritic spines (Fig. 4 E). Furthermore, overexpression of N-PBA failed to increase PSD-95–positive spines in hippocampal neurons, and C-PBA even resulted in a decrease of PSD-95–positive spine number (Fig. S4 H).

To test the hypothesis that GRK5 mediates actin bundling and links the bundled actin filaments to the PI(4,5)P2-enriched membrane, we examined the samples containing PI(4,5)P2-rich vesicles, F-actin, and a GRK5 variant by immunofluorescent microscopy. As shown in Fig. 4 F, both GRK5 and N-PBA induced visible actin bundles. Although phosphatidylcholine (PC) vesicles were randomly distributed and showed no apparent colocalization or association with actin bundles, ~90% of PI(4,5)P2-containing liposomes were distributed along with the actin bundles formed in the presence of GRK5. Furthermore, the capability of F-actin bundles to associate with PI(4,5)P2 liposomes was markedly reduced when incubated with N-PBA instead of WT GRK5 (Fig. 4 F). These data further indicate that, in addition to bundling actin through its C-terminal domain, GRK5 binds to PI(4,5)P2 via its N-terminal domain and, thus, targets the F-actin bundles to the membrane. Collectively, our results suggest that GRK5 promotes filopodial protrusion and dendritic development via coordinated actin bundling and PI(4,5)P2 binding.

GRK5 regulates dendritic development in vivo

To demonstrate the in vivo role of GRK5 in neuronal morphogenesis, a GRK5 RNAi–GFP construct was in utero electroporated into neuron progenitors at the ventricular zone of embryonic day 15.5 (E15.5) mice (Fig. S5 A). The migration of RNAi-GFP–positive cortical progenitors at the striatum level in the neocortex (mainly the somatosensory cortex) was observed. As shown in Fig. S5 B, the proportions of GRK5 RNAi–GFP-expressing cells among different cortical platelayers were not significantly different on P0 or P3 from those transfected with the control RNAi plasmid. However, examination of GRK5 RNAi–expressing neurons that had migrated to layer II/III on P7 indicated that these neurons possessed fewer and shorter dendritic branches compared with those transfected with control RNAi (Fig. 5, A–C). Furthermore, these defects in dendritic development caused by GRK5 RNAi could be rescued by cotransfection of bovine GRK5 and K215R but not by N-PBA or C-PBA (Fig. 5, A–C). Consistently, overexpression of GRK5 promoted an outgrowth of multiple branched processes in migrating neurons in the intermediate zone, whereas normally, these neurons only have a tailing process and a nonbranched leading process. In contrast to what was observed with WT GRK5, a markedly impaired effect was observed in neurons expressing N-PBA or C-PBA (Fig. 5 D). These results demonstrate that GRK5 could regulate dendritic development in vivo and that both actin-binding/bundling activity and PI(4,5)P2-binding property of GRK5 are critically involved in this process (Fig. 5 E).

GRK5 knockout (KO) mice exhibit immature spine morphology and impaired learning and memory

We further examined the role of GRK5 on neuronal morphogenesis in vivo using WT and GRK5 KO mice. As shown in Fig. S5 (C and D), hippocampal neurons from GRK5 KO mice showed decreased neurite number and neurite length as compared with those from WT mice. The results of Golgi staining showed that, compared with WT mice, the density of mature, mushroom-shaped spines on the dendrites of hippocampal pyramidal neurons in GRK5 KO mice was significantly reduced (Fig. 6, A–C). As shown in Fig. S5 E, the cumulative spine head/neck ratio, a morphological index of spine maturity, was also significantly lower in hippocampal neurons from GRK5 KO mice compared with those from WT mice (1.38 ± 0.52 vs. 2.01 ± 0.77; $P < 0.001$). However, no obvious change in either the density of mushroom-shaped spines or the spine morphology was observed in the corpus striatum in GRK5 KO mice (Fig. S5, F–H).

Changes in the number, size, and shape of dendritic spines are associated with synaptic plasticity, which underlies cognitive functions, such as learning and memory (Lamprecht and LeDoux, 2004). Mice with targeted disruption of the GRK5 gene exhibited no abnormalities in locomotor, open field, and elevated plus maze tests (Fig. S5, I–M). However, in the Morris water maze test, GRK5 KO mice showed slower learning than WT mice in searching for the hidden platform ($F(1, 38) = 26.66$; $P < 0.001$, two-way analysis of variance [ANOVA]) and impaired spatial memory for the target quadrant (Fig. 6, D and E; and Fig. S5, N and O). In the novel object location preference task, WT mice showed a significant preference for the object placed in a novel location, whereas the GRK5 KO mice showed

transfected with GRK5-GFP were treated with 10 µM ionomycin or pretreated with 1 µM PAO for 5 min and then stimulated with 1 µM BK. Neurons coexpressing GRK5-GFP, Lyn11-FRB (Lyn), and CFP-FKBP-Inp54p (InP) or CFP-FKBP-Inp54p (D281A) were also observed after treatment with 100 nM rapamycin. (C) Neurons cotransfected with GFP after dissection and the indicated constructs were observed at DIV2. One-way ANOVA followed by Tukey–Kramer posthoc test. Red arrowheads indicate dynamic filopodia. (D and E) Hippocampal neuron cultures were transfected at DIV5 and observed at DIV8 (D) or transfected at DIV9 and observed at DIV17 (E). GFP was cotransfected with GRK5 variants to visualize dendritic spines. Values of 30–40 neurons from three independent cultures were analyzed. One-way ANOVA followed by Tukey–Kramer posthoc test. Boxed regions are enlarged below each image. (F) 0.5 µM Alexa Fluor 488–labeled polymerized F-actin was incubated with 10 µM phosphatidylcholine (PC)- or PI(4,5)P2 (PIP2)-containing liposomes in the presence of 2 µM GRK5 or N-PBA for 1 h and imaged by confocal microscopy. Arrowheads indicate the liposomes that associate with and distribute along the actin bundles. Values from six to eight randomly selected images were analyzed. Student's *t* test. Error bars indicate SEM. *, $P < 0.05$; **, $P < 0.01$; ***, $P < 0.001$. Ctrl, control. Bars: (A, D, and E) 10 µm; (B and C) 1 µm; (F) 5 µm.

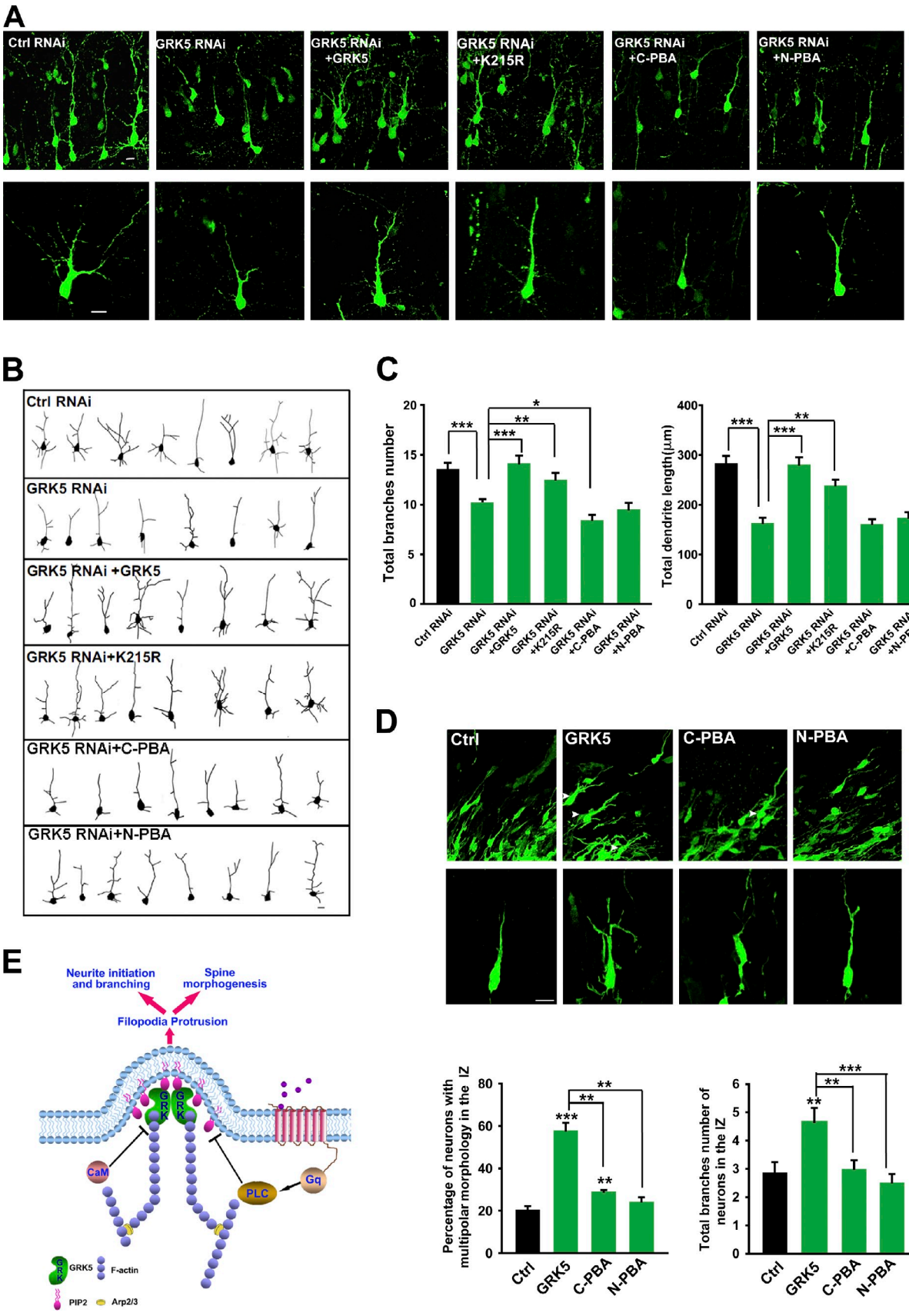

Figure 5. **GRK5 regulates dendritic development in vivo.** (A–C) Mouse embryos were electroporated in utero at E15.5 with the indicated plasmids, and brain sections were prepared on P7 and stained with GFP antibody to visualize transfected neurons. (A) Confocal images of GFP-positive neurons in layer II/III of the somatosensory cortex. Higher magnification images are shown below. (B) Reconstructions of cortical neurons using Neurolucida. (C) Total dendritic branch number and length of cortical neurons of 70–100 neurons from ≤5 to 10 brains. One-way ANOVA followed by Tukey–Kramer posthoc test.

no preference (Fig. 6 F). These data suggest that ablation of GRK5 impairs hippocampus-dependent memories. Consistently, the results from the recognition memory test showed that GRK5 KO mice are deficient in long-term recognition memory, which requires hippocampal synaptic plasticity (Fig. 6 G).

Discussion

Studies on the physiological function of GRKs have been primarily focused on their role of phosphorylating and desensitizing GPCRs in the past two decades. The present study found that overexpression of GRK5 promotes dendrite branching and spine maturation, whereas GRK5 deficiency leads to decreased dendrite branching and immature dendritic spines. Interestingly, this function of GRK5 does not depend on its kinase activity because the enhancement of dendrite branching and spine maturation could be replicated by a kinase-dead mutant of GRK5. Rather, dendrite branching and spine maturation were dependent on actin-bundling activity and phospholipid-binding property to promote filopodial protrusion. We showed that uncoupling GRK5-mediated actin and membrane dynamics by disruption of either the lipid-binding or actin-bundling property of GRK5 decreased the number and motility of dendritic filopodia, reduced dendrite branching, and led to fewer morphologically mature spines. Consistent with the critical effect of GRK5 on spine morphology in hippocampal neurons, GRK5 KO mice exhibited impaired spatial learning and memory and deficient long-term memory of object recognition. Our findings reveal GRK5 as a critical mediator of dendritic development and also indicate that coordinated actin cytoskeleton and membrane remodeling mediated by bifunctional actin-bundling and membrane-targeting molecules, such as GRK5, is crucial for proper neuronal morphogenesis and the establishment of functional neuronal circuitry.

Proteins bundling F-actin are involved in filopodial formation, which is required for many aspects of neuronal morphogenesis, including neurite initiation, dendrite branching, and spine formation (Gallo and Letourneau, 2004; Yuste and Bonhoeffer, 2004; Dent et al., 2007; Kwiatkowski et al., 2007). Our data revealed that GRK5 is colocalized with F-actin in the filopodia of growth cones in neurons, and it promotes filopodial formation, neurite initiation, dendrite branching, and spine formation. GRK5 has been shown in vitro to be capable of interacting with actin (Freeman et al., 1998). Our biochemical examinations further revealed that GRK5 acts as an actin-bundling protein during neuronal morphogenesis. Expression of C-PBA, the F-actin binding/bundling–deficient mutant of GRK5, decreased the number of dendritic branching, dendrite length, and mature spines in cultured neurons. These results demonstrate that GRK5 regulates filopodial formation and neuronal morphogenesis, and the F-actin–bundling activity of GRK5 is critically involved in the process.

In addition to the critical role of actin cytoskeleton regulation in the genesis of filopodia, recent studies revealed that BAR (Bin/amphiphysin/Rvs) domain–containing proteins, which are capable of forming a homodimer to interact with lipid bilayers via clusters of positively charged residues on their surface, can directly mold the plasma membrane in conjunction with actin remodeling and facilitate filopodial formation (Scita et al., 2008; Carlson and Soderling, 2009; Guerrier et al., 2009). These studies suggest that efficient deformation and extension of these membrane structures requires coordinated membrane remodeling and actin dynamics. The N terminus of GRK5 is able to specifically interact with the membrane phospholipid PI(4,5)P2 to target GRK5 to appropriate receptor substrates (Pitcher et al., 1996). Interestingly, we found that the effects of GRK5 on filopodial dynamics and neuronal morphogenesis are also crucially dependent on its interaction with PI(4,5)P2. Depletion of PI(4,5)P2 or mutating the PI(4,5)P2 binding site of GRK5 significantly impaired GRK5-promoted filopodia dynamics and neuronal morphogenesis. The fact that GRK5 can interact with PI(4,5)P2 and F-actin through separate domains lead us to postulate that GRK5 may function as a scaffold and linker between F-actin and plasma membrane enriched in PI(4,5)P2 to coordinate actin dynamics and membrane remodeling.

PI(4,5)P2 is an important phospholipid involved in actin dynamics. It is turned over locally in response to extracellular signals, such as thrombin, and is critical for the regulation of membrane cytoskeleton interactions (Tolias et al., 2000; Janmey and Lindberg, 2004). The N-terminal PI(4,5)P2 binding domain of GRK5 may act as a sensor for targeting and redistributing GRK5 to actin high dynamic structures stimulated by locally increased PI(4,5)P2 in response to extracellular signals. In this context, GRK5 may form dimers or oligomers, cross-link F-actin into bundles through its C-terminal F-actin binding domain, and target the bundled actin to the PI(4,5)P2-rich membrane through its N-terminal PI(4,5)P2 binding domain. This would facilitate filopodial protrusion and allows morphological changes from actin cytoskeleton remodeling to occur at appropriate sites of the plasma membrane. We have shown that this process is regulated by calmodulin through direct competition with F-actin for GRK5. This dual role of GRK5 in membrane remodeling and actin cytoskeleton dynamics that link bundled actin filaments to specific membrane phospholipids may represent a new model to comprehend the complex molecular mechanism of filopodial formation (Fig. 5 E). Our results

(D) Embryos were electroporated in utero at E15.5 with indicated plasmids, and brain sections were prepared on E17.5 and stained with GFP antibody for visualization of transfected neurons. Shown are images of GFP-positive neurons in the intermediate zone. Arrowheads indicate neurons with at least three processes. Data plotted are percentages of neurons with at least three processes and total branch number quantified from 180–400 neurons from three brains. IZ, intermediate zone. One-way ANOVA followed by Tukey–Kramer posthoc test. (E) Cartoon for the proposed model of GRK5-regulated neuronal morphogenesis. GRK5 forms dimers or oligomers to cross-link F-actin into bundles through its C-terminal F-actin binding domain and target the bundled actin to a PI(4,5)P2 (PIP2)-rich membrane through its N-terminal PI(4,5)P2 binding domain. This facilitates filopodial protrusion, neurite initiation and branching, and spine morphogenesis. This process could be regulated by Ca^{2+}/calmodulin through its direct competition with F-actin for binding to GRK5 and by Gαq-coupled receptors through PLC-stimulated PI(4,5)P2 turnover. Error bars represent means ± SEM. *, $P < 0.05$; **, $P < 0.01$; ***, $P < 0.001$. Ctrl, control. Bars, 10 µm.

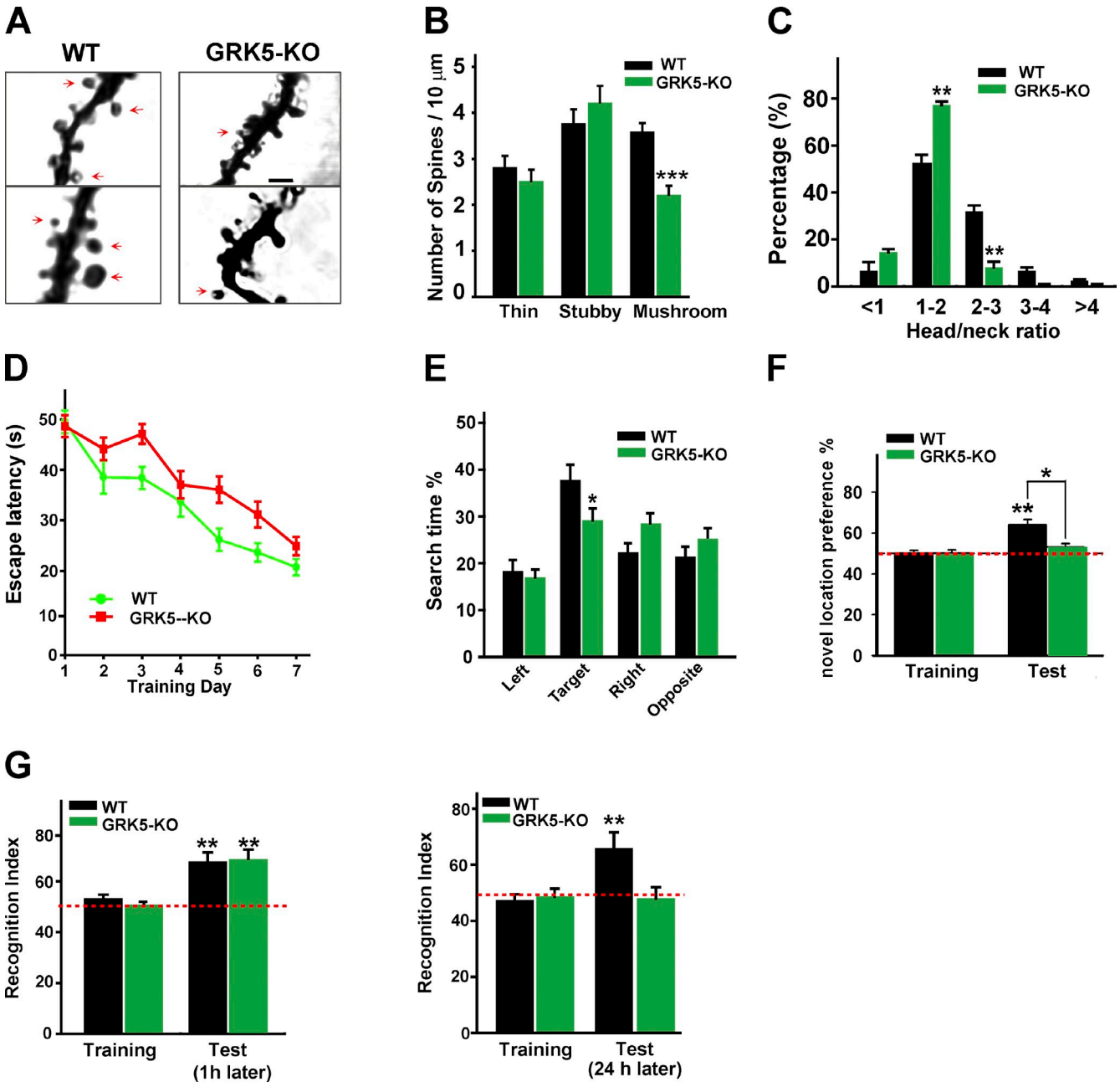

Figure 6. **GRK5 KO mice exhibit immature spine morphology and impaired learning and memory.** (A–C) Morphological analysis of hippocampal neurons. (A) Confocal images of dendritic spines of pyramidal neuron in Golgi-stained hippocampal slices. Arrows indicate typical dendritic spines. (B and C) Quantification of number and head/neck ratios of spines randomly selected from the apical dendrites (n = 200–250) of hippocampal pyramidal neurons from adult WT (n = 3) and GRK5 KO (n = 4) mice. **, $P < 0.01$; ***, $P < 0.001$ versus WT (Student's t test). Bar, 2 µm. (D and E) Morris water maze test. (D) The escape latency for hidden platform during the consecutive 7-d training ($F(1,38) = 26.66$; $P < 0.001$, two-way ANOVA). (E) Searching time in left, target, right, and opposite quadrants during the probe test conducted on day 8. WT, n = 18; GRK5 KO, n = 22. *, $P < 0.05$ versus WT (Student's t test). (F) Novel object location preference task. GRK5 KO mice (n = 17) and WT mice (n = 15) were subjected to a 1 h-delay object location test. The percentage of time spent exploring the object that has been moved to a novel location was calculated. GRK5 KO mice showed impaired novel location preference. **, $P < 0.01$ as compared with the chance level (50%); *, $P < 0.05$, compared with WT (Student's t test). (G) Object recognition test. Mice were tested 1 or 24 h after training. The percentage of time spent exploring the novel object was calculated. The red dotted line indicates a 50% chance level. WT, n = 15; GRK5 KO, n = 17. **, $P < 0.01$ versus the chance level (50%; Student's t test). Error bars indicate SEM.

further support the hypothesis that efficient membrane protrusion requires the coordination of multiple mechanisms, including membrane remodeling and actin dynamics (Scita et al., 2008; Carlson and Soderling, 2009), and identify GRK5 as a key linker to guide bundled actin to membranes to promote neuronal morphogenesis.

Spine shape and volume are determined mostly by the F-actin cytoskeleton and are correlated with the strength and maturity of each spine synapse. Appropriate spine morphology is particularly important for synaptic plasticity and adaptive behaviors. In this study, we showed that GRK5 KO mice exhibit immature spine morphology, impaired spatial learning and

memory, and a defect in long-term object recognition memory. These results indicate that the regulation of neuronal morphogenesis by GRK5 is crucial for appropriate neuronal development and brain function. Many GPCRs have been implicated in regulating neurological and behavioral processes, such as learning and memory (Catapano and Manji, 2007). Although the specificity and physiological consequence of GRK5-regulated GPCR signaling in the brain are largely unknown, the possibility that regulation of GPCR signaling by GRK5-catalyzed phosphorylation may also contribute to the learning and memory phenotypes seen in GRK5 KO mice could not be excluded. It is likely that GRK5 regulates cell physiology and brain functions by multiple mechanisms: as a kinase to phosphorylate and desensitize GPCR signaling and as a scaffold to regulate non-GPCR proteins noncatalytically, such as in the case of F-actin and PI(4,5)P2. We are in the process of making K215R knockin mice to examine the kinase activity–dependent and –independent functions of GRK5 in vivo.

Materials and methods

Plasmid construction

Plasmids encoding tagged bovine GRK5 or its mutants were constructed by PCR mutagenesis. The microRNA (miRNA)-based RNAi system, which uses the pcDNA 6.2-gateway/Emerald GFP (EmGFP)-miRNA vector to enable simultaneous expression of the EmGFP protein and miRNA, was purchased from Invitrogen. The protein level of EmGFP corresponds to the expression of miRNA. *LacZ* RNAi (Invitrogen) was used as a control. Sequences for GRK5 RNAi are rat, 5′-TGCTGTTCAGTTCTAGTTAGGATGCTGTTTTGGCCACTGACTGACAGCATCCTCTAGAACTGAA-3′ (sense) and 5′-CCTGTTCAGTTCTAGAGGATGCTGTCAGTCAGTGGCCAAAACAGCATCCTAACTAGAACTGAAC-3′ (antisense); and mouse, 5′-TGCTGTTGAGTAGAAGTCATCGTCCGGTTTTGGCCACTGACTGACCGGACGATCTTCTACTCAA-3′ (sense) and 5′-CCTGTTGAGTAGAAGATCGTCCGGTCAGTCAGTGGCCAAAACCGGACGATGACTTCTACTCAAC-3′ (antisense). The mCherry actin plasmid was provided by D.A. Applewhite (University of North Carolina, Chapel Hill, NC). Lyn, Inp, and CFP-FKBP-Inp54p (D281A) plasmids were provided by T. Meyer (Stanford University Medical School, Stanford, CA).

Reagents and antibodies

Modified Eagle's medium and DME were purchased from Invitrogen. FBS was obtained from Hyclone. Mouse anti–β-tubulin antibody, rabbit and mouse antibodies against the Flag epitope, and rabbit antibodies against the HA epitope were purchased from Sigma-Aldrich. Cy3-conjugated goat anti–rabbit/anti–mouse and Cy5-conjugated goat anti–mouse IgG were purchased from Jackson ImmunoResearch Laboratories, Inc. Alexa Fluor 488–labeled rabbit muscle globular actin (G-actin), Alexa Fluor 546–labeled phalloidin (F-actin), and TRITC DHPE (*N*-(6-teramethylrhodamine-thio-carbamoyl)-1,2-dihexadecanoyl-*sn*-glycero-3-phosphoethanolamine, triethylammonium salt) were obtained from Invitrogen. The mouse anti–PSD-95 antibody was purchased from Millipore. Goat polyclonal antibodies against GRK5 were obtained from R&D Systems (AF4539). Mouse polyclonal antibodies against GRK5 (G-2) were raised by immunizing BALB/c mice with purified bovine GRK5-Flag.

Cell culture and plasmid transfection

HEK293T cells were cultured in DME containing 10% FBS. Cells were seeded in 60- or 100-mm tissue-culture dishes at 0.6–2 × 10^6/dish 20 h before transfection. Cells were transfected with 2–5 µg of each plasmid using the calcium phosphate/DNA coprecipitation method. Assays were performed 44–48 h after transfection. Neuro-2a cells were cultured in modified Eagle's medium plus 10% FBS and were transfected using Lipofectamine 2000 reagent (Invitrogen) according to the manufacturer's instructions.

Hippocampal neuron culture and transfection

Cultures of hippocampal neurons were prepared from Sprague-Dawley rats of P0. After treatment with 0.1 mg/ml trypsin (Invitrogen) and 0.6 µg/ml DNase (Sigma-Aldrich) for 15 min at 37°C and mechanical dissociation, hippocampal cells were plated at 50,000 cells/cm^2 on 8-mm coverslips coated with 0.1 mg/ml poly-DL-lysine. The cells were cultured in neurobasal medium containing 2 mM glutaMAX, 1% penicillin-streptomycin, and B27 supplement (Invitrogen) in 5% CO_2/10% O_2 atmosphere at 37°C. The hippocampal neurons were transiently transfected at DIV5 or DIV9 using the calcium phosphate method (Köhrmann et al., 1999). DIV1 neurons were electroporated by nucleofection as described by the manufacturer (Lonza). In brief, 2 × 10^6 neurons were suspended with 4 µg DNA in the nucleofection solution provided. Cells were plated at a final density of 200,000/cm^2 and allowed to recover in DME with 10% calf serum for 1 h before replacement with B27-supplemented neurobasal medium.

In utero electroporation

Plasmids were transfected using intraventricular injection followed by in utero electroporation (Kawauchi et al., 2003, 2006; Wang et al., 2007). In brief, C57BL/6J mice at 15.5 d of gestation were anesthetized with 10% chloral hydrate (4 ml/kg of body weight). 1–2 µl miRNA-based RNAi plasmids mixed with 2 mg/ml Fast Green (Sigma-Aldrich) were injected by trans-uterus pressure microinjection into the lateral ventricle of embryos. Then, electric pulses generated by a square wave electroporation system (ElectroSquireportator T830; BTX) were applied to the cerebral wall at five repeats of 28 V for 50 ms with an interval of 950 ms.

Immunostaining and Golgi staining

Cultures of hippocampal neurons, Neuro-2a cells, and HeLa cells were fixed with 3.7% formaldehyde, permeabilized in 0.1% Triton X-100, and blocked. Then, they were incubated with primary (1:50–1:200 dilution) and appropriate secondary antibodies (1:200 dilution). Postnatal mice brains were removed and fixed in 4% paraformaldehyde overnight after transcardial perfusion. After dehydration in 20% glucose, brains were cut at coronal cryostat sections of 50 µm. Sections were processed for immunostaining by a three-step free-floating protocol. Anti-GFP (Invitrogen), biotinylated anti–rabbit IgG, and Cy2-conjugated streptavidin (Rockland Immunochemicals, Inc.) were used for staining. For Golgi staining, brains were rapidly isolated and fixed in 10% formalin for 24 h. After being immersed in 3% potassium dichromate for 5 d in the dark, the fixed brains were treated further in 2% silver nitrate for 48 h, and the vibration sections were cut at 40 µm.

Image acquisition and morphological analysis

Fixed cells and brain section images were acquired at room temperature using a confocal microscope (LSM 510; Carl Zeiss) with a 40 or 63× oil objective (Carl Zeiss) and arranged using Photoshop software (Adobe). Frame scans of fluorescence intensity were performed using the intensity profile function of the software (LSM 510). For morphological analysis, the z-series stacks of confocal images (5–10 optical sections were collected at 0.5-µm intervals) were semiautomatically traced using the software Neurolucida (MicroBrightField, Inc.). The total length and branch number of each individual process in transfected neurons were analyzed using the program Neuroexplorer (Nex Technologies). Dendritic protrusions ≥10 µm were identified as branches and were statistically included. Dendritic protrusions <10 µm were identified as filopodia. Other morphological analysis was performed using Image-Pro Plus 5.1 software (Media Cybernetics). For neuron migration, EGFP-labeled cortical neurons on brain sections were counted across three different cortical zones at different developmental stages, and the distribution of transfected cortical neurons was analyzed. For branch tip number, tips of all axonal or dendritic protrusions >10 µm were manually counted. For the number of dendritic protrusions, the proximal dendrites (identified as processes extending from the neuronal cell body and ≥1 µm in diameter) were selected. Dendritic protrusions <3 µm in length showing visible spine heads or positives for PSD-95 immunoactivity were quantified. Thin protrusions without enlargement were defined as filopodia-like protrusions. For the ratio of the average immunofluorescence intensity between the spine head and the dendritic shaft, images were measured on manually selected spine head and dendritic shaft areas. Time-lapse experiments were performed using a laser-spinning disc confocal system (UltraVIEW; PerkinElmer). Cells growing on glass coverslips with culture mediums were visualized at 37°C under an inverted microscope (IX81-ZDC; Olympus) with a 60×, 1.42 NA objective. Images were acquired by UltraVIEW software using a high-resolution digital charge-coupled device camera (EMCCD C9100-13; Hamamatsu Photonics) at 10-s intervals.

High-speed sedimentation F-actin–binding assays

Bovine GRK5-Flag or mutants were purified from HEK293T cells. In brief, HEK293T cells overexpressing GRK5-Flag or mutants were lysed in lysis

buffer (50 mM Tris, pH 7.4, 250 mM NaCl, 1% Triton X-100, 10% glycerol, and 2 mM EDTA plus 10 µg/ml aprotinin, 10 µg/ml benzamidine, and 0.2 mM PMSF). After centrifugation, proteins were immunoprecipitated with M2-conjugated Sepharose (Sigma-Aldrich). After extensive washing in lysis buffer, beads were rinsed by TBS (50 mM Tris, pH 7.4, and 50 mM NaCl) twice. Bound protein was eluted by a competition with the 3×Flag peptide (Sigma-Aldrich) as the product instructions suggested. The 3×Flag peptide and salt were removed by centrifugation in a centrifugal filter unit (30-kD cutoff size; Amicon Ultra-4; Millipore). Protein purity was determined by 10% SDS-PAGE. Rabbit muscle G-actin was purchased from Cytoskeleton. G-actin was maintained in G buffer (5 mM Tris-Cl, pH 8.0, 0.2 mM ATP, 0.5 mM DTT, and 0.2 mM $CaCl_2$). ATP–G-actin was polymerized at room temperature for 1 h in 50× F buffer (50 mM KCl, 10 mM Tris, pH 7.5, 0.2 mM DTT, 2 mM $MgCl_2$, and 0.2 mM ATP). Concentration measures given for F-actin in this paper refer to the initial concentration of G-actin before polymerization. For binding assays, purified proteins were clarified by centrifugation at 350,000 *g* for 30 min at 4°C to remove any aggregates. 1 µM purified proteins were incubated with a range of concentrations (0–8 µM) of F-actin or 2.5 µM F-actin in 50× F buffer for 30 min on ice and then centrifuged at 350,000 *g* for 30 min at 4°C. Supernatants were removed, and pellets were rinsed with F buffer and then resuspended in a volume of 50× F buffer equal to that of the supernatant. Equal aliquots of supernatants and pellets of samples were analyzed by SDS-PAGE and Coomassie blue staining and quantified by Image-Pro Plus 5.1 software.

Fluorescence microscopy of actin bundling and low-speed sedimentation

F-actin–bundling assay

Alexa Fluor 488–labeled rabbit muscle G-actin was purchased from Invitrogen. 50% labeled G-actin was maintained in G buffer. 4 µM ATP–G-actin was polymerized in the presence of various purified proteins in 100× F buffer (100 mM KCl, 10 mM Tris, pH 7.5, 0.2 mM DTT, 2 mM $MgCl_2$, and 0.2 mM ATP) for 1 h at room temperature, or polymerized 50% labeled F-actin (4 µM) was incubated with purified proteins for 1 h at room temperature in 100× F buffer. The samples were then mounted between a slide and coverslip and imaged by confocal microscopy. For the low-speed sedimentation actin-bundling experiment, purified proteins were incubated with the indicated concentrations of F-actin (0–8 µM) in 100× F buffer at room temperature for 1 h and then centrifuged at 10, 000 *g* for 30 min at room temperature. Supernatants and pellets were analyzed by SDS–PAGE and Coomassie Blue staining and quantified by Image-Pro Plus 5.1 software.

Visualization of association of F-actin with liposomes

PI(4,5)P2 (porcine brain triammonium salt) and PC (brain) were purchased from Avanti Polar Lipids, Inc. PC, PI(4,5)P2, and TRITC DHPE were dissolved in chloroform. PI(4,5)P2 or PC containing 2% TRITC DHPE in chloroform was vacuum dried onto a round-bottom flask by rotary evaporation for 2 h at room temperature and hydrated at 37°C for 1 h with vesicle buffer (50 mM NaCl/10 mM Tris, pH 7.5) containing 5% (wt/wt) sucrose to a total lipid concentration of 0.5 mM. Polymerized Alexa Fluor 488–labeled F-actin (0.5 µM) was incubated in the presence of 2 µM GRK5 or N-PBA and 10 µM PC- or PI(4,5)P2-containing liposomes in 50× F buffer for 1 h at room temperature. The samples were then mounted and imaged by confocal microscopy.

Animals

GRK5 KO mice were provided by R.J. Lefkowitz and R.T. Premont (Duke University Medical Center, Durham, NC). GRK5 KO mice and their WT littermates were obtained from self-crossing GRK5 heterozygous mice. Genotypes of the mice were determined by PCR amplification using tail tip DNA as previously described (Gainetdinov et al., 1999; Walker et al., 2004). The mRNA from mice were also obtained and reverse transcribed to cDNA for PCR amplification using primers specially located at the GRK5 exon 7 and exon 8 locus (sense, 5′-AGGTTCGGGCCACTGGTA-3′, and antisense, 5′-ATTCGCCTTTCCTCTTTT-3′). Mice were housed in groups and maintained on a 12-h light/dark cycle with food and water available ad libitum. The experiments were conducted on dark phase. All procedures conformed to the National Institutes of Health Guide for the Care and Use of Laboratory Animals.

Locomotor activity and open field tests

An activity monitor system (43.2 × 43.2 × 30.5 cm; Open Field Activity Chamber MED-OFA-MS; Med Associates, Inc.) was used to detect horizontal movement. In brief, this system uses paired sets of photo beams to detect movement in the open field, and movement is recorded as beam breaks. Each mouse was placed in the center of the open field and explored freely for 60 min. The total distance traveled was recorded as locomotor activity. The center area entries and time spent were recorded as an anxiety-related parameter.

Elevated plus maze test

The elevated plus maze consisted of a center platform and four arms (34.5-cm length × 6.3-cm width × 19.5-cm height) placed 75 cm above the floor. Two arms were enclosed within walls (closed arms), and the other two had low rims (open arms). Mice were placed in the center, and their behaviors were recorded for 5 min with a camera (B5; Uni Flying) located above the maze. Time spent and entries in the different compartments (closed and open arms in the center) were assessed. The arms were cleaned thoroughly between each test to ensure the absence of olfactory cues.

Morris water maze

The water maze was a gray circle pool that was 120 cm in diameter and 50 cm in height. The water filled with defatted milk was kept at 21 ± 1°C. A submerged circle platform (10 cm in diameter and 1 cm beneath water surface) was located at a fixed location through the whole training trial and removed in the probe test. The hidden platform training consisted of four trials (maximum time of 60 s and intertrial interval of 20 min) each day for a consecutive 7 d. The average escape latencies to find the submerged platform of each trial were obtained and averaged for each day of acquisition. A single 60-s probe test was administrated on day 8 with the platform removed. The trajectories of the mice were recorded with a video camera (B5), and the percent of time spent in each quadrant was calculated for memory retention. Data represent means ± SEM. Another set of mice were used for visible platform training. The training consisted of four trials (maximum time of 60 s and intertrial interval of 20 min) each day for a consecutive 3 d. The average escape latencies of each trial were obtained and averaged for each trail of acquisition.

Object recognition task

The exploration arena was an open-topped box (60 × 60 × 40 cm; made of gray-painted wood with a floor covered with sawdust) placed in a dimly illuminated room. Object A was a glass cube, and object B was a plastic cylinder. They were cleaned thoroughly between training to ensure the absence of olfactory cues. The procedure consisted of a training phase and a preference test phase after a delay of 1 or 24 h. Mice were initially allowed to explore the box for 20 min for habitation before training. In the training phase, mice were subjected to two blocks of 10-min trials, with a 10-min interval between blocks. In each trial, they were allowed to explore two of the same copies of object A (A_1 and A_2) placed in diagonal corners of the arena (10 cm from each adjacent wall). In the test phase, A_1 was substituted by another copy, A_3, and A_2 was substituted by object B (novel object) placed in the original position. During the interval, the mice were placed in the holding cage in the room. The time for exploring the objects (nose pointing toward the object at a distance ≤1 cm) in training phase and test phase was recorded. The object recognition index was calculated as $T_{A2}/(T_{A1} + T_{A2})$ in training phase or $T_B/(T_{A3} + T_B)$ in test phase.

Object location preference experiment

The exploration arena was an open-topped box (40 × 40 × 40 cm; made of wood) with different spatial cues attached on three walls to indicate different directions. The training and test intervals were similar to those for the object recognition task. In the preference test, two of the same copies (A3 and A4) were substituted: one (A3) placed in the same position as A1 and another (A4) placed in the corner adjacent to the original position of A2 (referred to as the novel location). The exploration time was 5 min. The time spent to explore every object in the training phase and test phase was recorded. Object location preference index was calculated as $T_{A2}/(T_{A1} + T_{A2})$ in training phase or $T_{A4}/(T_{A3} + T_{A4})$ in test phase.

Online supplemental material

Fig. S1 shows that GRK5 regulates neuritogenesis and dendritic development. Fig. S2 shows that GRK5 is colocalized with F-actin at sites of actin high dynamic structures. Fig. S3 shows that C-terminal basic residues of GRK5 are essential for its binding to F-actin and self-interaction of GRK5. Fig. S4 shows that C-terminal and N-terminal basic residues of GRK5 are critical for its effect on filopodia dynamics and dendritic development. Fig. S5 shows the effects of depletion of GRK5 in vivo on neuronal migration, spine morphology, and learning and memory. Online supplemental material is available at http://www.jcb.org/cgi/content/full/jcb.201104114/DC1.

We thank Drs. D.A. Applewhite for the mCherry actin plasmid, T. Meyer for Lyn, Inp, and CFP-FKBP-Inp54p (D281A) constructs, R.J. Lefkowitz and R.T. Premont for GRK5 KO mice, and G. Pei, X. Yu, S. Duan, and Y. Ding for comments and technical support.

This research was supported by the Ministry of Science and Technology grant 2009CB522006 (to L. Ma) and National Natural Science Foundation of China grants 30830042 and 30821002 (to L. Ma), 30800646 (to H. Long), 30900438 (to F. Wang), and 30900852 (to Y. Chen).

Submitted: 21 April 2011
Accepted: 22 August 2011

References

Ahmari, S.E., and S.J. Smith. 2002. Knowing a nascent synapse when you see it. *Neuron*. 34:333–336. http://dx.doi.org/10.1016/S0896-6273(02)00685-2

Burnette, D.T., A.W. Schaefer, L. Ji, G. Danuser, and P. Forscher. 2007. Filopodial actin bundles are not necessary for microtubule advance into the peripheral domain of Aplysia neuronal growth cones. *Nat. Cell Biol.* 9:1360–1369. http://dx.doi.org/10.1038/ncb1655

Carlson, B., and S.H. Soderling. 2009. Mechanisms of cellular protrusions branch out. *Dev. Cell*. 17:307–309. http://dx.doi.org/10.1016/j.devcel.2009.08.015

Carman, C.V., J.L. Parent, P.W. Day, A.N. Pronin, P.M. Sternweis, P.B. Wedegaertner, A.G. Gilman, J.L. Benovic, and T. Kozasa. 1999. Selective regulation of Galpha(q/11) by an RGS domain in the G protein-coupled receptor kinase, GRK2. *J. Biol. Chem.* 274:34483–34492. http://dx.doi.org/10.1074/jbc.274.48.34483

Catapano, L.A., and H.K. Manji. 2007. G protein-coupled receptors in major psychiatric disorders. *Biochim. Biophys. Acta*. 1768:976–993. http://dx.doi.org/10.1016/j.bbamem.2006.09.025

Dailey, M.E., and S.J. Smith. 1996. The dynamics of dendritic structure in developing hippocampal slices. *J. Neurosci.* 16:2983–2994.

da Silva, J.S., and C.G. Dotti. 2002. Breaking the neuronal sphere: regulation of the actin cytoskeleton in neuritogenesis. *Nat. Rev. Neurosci.* 3:694–704. http://dx.doi.org/10.1038/nrn918

Dent, E.W., A.M. Barnes, F. Tang, and K. Kalil. 2004. Netrin-1 and semaphorin 3A promote or inhibit cortical axon branching, respectively, by reorganization of the cytoskeleton. *J. Neurosci.* 24:3002–3012. http://dx.doi.org/10.1523/JNEUROSCI.4963-03.2004

Dent, E.W., A.V. Kwiatkowski, L.M. Mebane, U. Philippar, M. Barzik, D.A. Rubinson, S. Gupton, J.E. Van Veen, C. Furman, J. Zhang, et al. 2007. Filopodia are required for cortical neurite initiation. *Nat. Cell Biol.* 9:1347–1359. http://dx.doi.org/10.1038/ncb1654

Dierssen, M., and G.J. Ramakers. 2006. Dendritic pathology in mental retardation: from molecular genetics to neurobiology. *Genes Brain Behav.* 5(Suppl. 2):48–60. http://dx.doi.org/10.1111/j.1601-183X.2006.00224.x

Doherty, G.J., and H.T. McMahon. 2008. Mediation, modulation, and consequences of membrane-cytoskeleton interactions. *Annu Rev Biophys*. 37:65–95. http://dx.doi.org/10.1146/annurev.biophys.37.032807.125912

Fiala, J.C., J. Spacek, and K.M. Harris. 2002. Dendritic spine pathology: cause or consequence of neurological disorders? *Brain Res. Brain Res. Rev.* 39:29–54. http://dx.doi.org/10.1016/S0165-0173(02)00158-3

Freeman, J.L., E.M. De La Cruz, T.D. Pollard, R.J. Lefkowitz, and J.A. Pitcher. 1998. Regulation of G protein-coupled receptor kinase 5 (GRK5) by actin. *J. Biol. Chem.* 273:20653–20657. http://dx.doi.org/10.1074/jbc.273.32.20653

Gainetdinov, R.R., L.M. Bohn, J.K. Walker, S.A. Laporte, A.D. Macrae, M.G. Caron, R.J. Lefkowitz, and R.T. Premont. 1999. Muscarinic supersensitivity and impaired receptor desensitization in G protein-coupled receptor kinase 5-deficient mice. *Neuron*. 24:1029–1036. http://dx.doi.org/10.1016/S0896-6273(00)81048-X

Gallo, G., and P.C. Letourneau. 1998. Axon guidance: GTPases help axons reach their targets. *Curr. Biol.* 8:R80–R82. http://dx.doi.org/10.1016/S0960-9822(98)70051-X

Gallo, G., and P.C. Letourneau. 2004. Regulation of growth cone actin filaments by guidance cues. *J. Neurobiol.* 58:92–102. http://dx.doi.org/10.1002/neu.10282

Guerrier, S., J. Coutinho-Budd, T. Sassa, A. Gresset, N.V. Jordan, K. Chen, W.L. Jin, A. Frost, and F. Polleux. 2009. The F-BAR domain of srGAP2 induces membrane protrusions required for neuronal migration and morphogenesis. *Cell*. 138:990–1004. http://dx.doi.org/10.1016/j.cell.2009.06.047

Gupton, S.L., and F.B. Gertler. 2007. Filopodia: the fingers that do the walking. *Sci. STKE*. 2007:re5. http://dx.doi.org/10.1126/stke.4002007re5

Janmey, P.A., and U. Lindberg. 2004. Cytoskeletal regulation: rich in lipids. *Nat. Rev. Mol. Cell Biol.* 5:658–666. http://dx.doi.org/10.1038/nrm1434

Jiang, X., P. Yang, and L. Ma. 2009. Kinase activity-independent regulation of cyclin pathway by GRK2 is essential for zebrafish early development. *Proc. Natl. Acad. Sci. USA*. 106:10183–10188. http://dx.doi.org/10.1073/pnas.0812105106

Kawauchi, T., K. Chihama, Y. Nabeshima, and M. Hoshino. 2003. The in vivo roles of STEF/Tiam1, Rac1 and JNK in cortical neuronal migration. *EMBO J.* 22:4190–4201. http://dx.doi.org/10.1093/emboj/cdg413

Kawauchi, T., K. Chihama, Y. Nabeshima, and M. Hoshino. 2006. Cdk5 phosphorylates and stabilizes p27kip1 contributing to actin organization and cortical neuronal migration. *Nat. Cell Biol.* 8:17–26. http://dx.doi.org/10.1038/ncb1338

Kohout, T.A., and R.J. Lefkowitz. 2003. Regulation of G protein-coupled receptor kinases and arrestins during receptor desensitization. *Mol. Pharmacol.* 63:9–18. http://dx.doi.org/10.1124/mol.63.1.9

Köhrmann, M., W. Haubensak, I. Hemraj, C. Kaether, V.J. Lessmann, and M.A. Kiebler. 1999. Fast, convenient, and effective method to transiently transfect primary hippocampal neurons. *J. Neurosci. Res.* 58:831–835. http://dx.doi.org/10.1002/(SICI)1097-4547(19991215)58:6<831::AID-JNR10>3.0.CO;2-M

Kwiatkowski, A.V., D.A. Rubinson, E.W. Dent, J. Edward van Veen, J.D. Leslie, J. Zhang, L.M. Mebane, U. Philippar, E.M. Pinheiro, A.A. Burds, et al. 2007. Ena/VASP is required for neuritogenesis in the developing cortex. *Neuron*. 56:441–455. http://dx.doi.org/10.1016/j.neuron.2007.09.008

Lamprecht, R., and J. LeDoux. 2004. Structural plasticity and memory. *Nat. Rev. Neurosci.* 5:45–54. http://dx.doi.org/10.1038/nrn1301

Lefkowitz, R.J. 2007. Seven transmembrane receptors: something old, something new. *Acta Physiol. (Oxf.)*. 190:9–19. http://dx.doi.org/10.1111/j.1365-201X.2007.01693.x

Levay, K., D.K. Satpaev, A.N. Pronin, J.L. Benovic, and V.Z. Slepak. 1998. Localization of the sites for Ca2+-binding proteins on G protein-coupled receptor kinases. *Biochemistry*. 37:13650–13659. http://dx.doi.org/10.1021/bi980998z

Luo, L. 2002. Actin cytoskeleton regulation in neuronal morphogenesis and structural plasticity. *Annu. Rev. Cell Dev. Biol.* 18:601–635. http://dx.doi.org/10.1146/annurev.cellbio.18.031802.150501

Métayé, T., H. Gibelin, R. Perdrisot, and J.L. Kraimps. 2005. Pathophysiological roles of G-protein-coupled receptor kinases. *Cell. Signal.* 17:917–928. http://dx.doi.org/10.1016/j.cellsig.2005.01.002

Newey, S.E., V. Velamoor, E.E. Govek, and L. Van Aelst. 2005. Rho GTPases, dendritic structure, and mental retardation. *J. Neurobiol.* 64:58–74. http://dx.doi.org/10.1002/neu.20153

Penzes, P. 2007. Pumping up the synapse. *Neuron*. 56:942–944. http://dx.doi.org/10.1016/j.neuron.2007.12.006

Pitcher, J.A., Z.L. Fredericks, W.C. Stone, R.T. Premont, R.H. Stoffel, W.J. Koch, and R.J. Lefkowitz. 1996. Phosphatidylinositol 4,5-bisphosphate (PIP2)-enhanced G protein-coupled receptor kinase (GRK) activity. Location, structure, and regulation of the PIP2 binding site distinguishes the GRK subfamilies. *J. Biol. Chem.* 271:24907–24913. http://dx.doi.org/10.1074/jbc.271.40.24907

Pollard, T.D., and G.G. Borisy. 2003. Cellular motility driven by assembly and disassembly of actin filaments. *Cell*. 112:453–465. http://dx.doi.org/10.1016/S0092-8674(03)00120-X

Premont, R.T., and R.R. Gainetdinov. 2007. Physiological roles of G protein-coupled receptor kinases and arrestins. *Annu. Rev. Physiol.* 69:511–534. http://dx.doi.org/10.1146/annurev.physiol.69.022405.154731

Pronin, A.N., D.K. Satpaev, V.Z. Slepak, and J.L. Benovic. 1997. Regulation of G protein-coupled receptor kinases by calmodulin and localization of the calmodulin binding domain. *J. Biol. Chem.* 272:18273–18280. http://dx.doi.org/10.1074/jbc.272.29.18273

Scita, G., S. Confalonieri, P. Lappalainen, and S. Suetsugu. 2008. IRSp53: crossing the road of membrane and actin dynamics in the formation of membrane protrusions. *Trends Cell Biol.* 18:52–60. http://dx.doi.org/10.1016/j.tcb.2007.12.002

Sorriento, D., M. Ciccarelli, G. Santulli, A. Campanile, G.G. Altobelli, V. Cimini, G. Galasso, D. Astone, F. Piscione, L. Pastore, et al. 2008. The G-protein-coupled receptor kinase 5 inhibits NFkappaB transcriptional activity by inducing nuclear accumulation of IkappaB alpha. *Proc. Natl. Acad. Sci. USA*. 105:17818–17823. http://dx.doi.org/10.1073/pnas.0804446105

Suetsugu, S., and T. Takenawa. 2003. Regulation of cortical actin networks in cell migration. *Int. Rev. Cytol.* 229:245–286. http://dx.doi.org/10.1016/S0074-7696(03)29006-9

Suh, B.C., T. Inoue, T. Meyer, and B. Hille. 2006. Rapid chemically induced changes of PtdIns(4,5)P2 gate KCNQ ion channels. *Science*. 314:1454–1457. http://dx.doi.org/10.1126/science.1131163

Tolias, K.F., J.H. Hartwig, H. Ishihara, Y. Shibasaki, L.C. Cantley, and C.L. Carpenter. 2000. Type Ialpha phosphatidylinositol-4-phosphate 5-kinase

mediates Rac-dependent actin assembly. *Curr. Biol.* 10:153–156. http://dx.doi.org/10.1016/S0960-9822(00)00315-8

van Rheenen, J., and K. Jalink. 2002. Agonist-induced PIP(2) hydrolysis inhibits cortical actin dynamics: regulation at a global but not at a micrometer scale. *Mol. Biol. Cell*. 13:3257–3267. http://dx.doi.org/10.1091/mbc.E02-04-0231

Walker, J.K., R.R. Gainetdinov, D.S. Feldman, P.K. McFawn, M.G. Caron, R.J. Lefkowitz, R.T. Premont, and J.T. Fisher. 2004. G protein-coupled receptor kinase 5 regulates airway responses induced by muscarinic receptor activation. *Am. J. Physiol. Lung Cell. Mol. Physiol.* 286:L312–L319. http://dx.doi.org/10.1152/ajplung.00255.2003

Wang, C.L., L. Zhang, Y. Zhou, J. Zhou, X.J. Yang, S.M. Duan, Z.Q. Xiong, and Y.Q. Ding. 2007. Activity-dependent development of callosal projections in the somatosensory cortex. *J. Neurosci.* 27:11334–11342. http://dx.doi.org/10.1523/JNEUROSCI.3380-07.2007

Yang, C., M. Hoelzle, A. Disanza, G. Scita, and T. Svitkina. 2009. Coordination of membrane and actin cytoskeleton dynamics during filopodia protrusion. *PLoS ONE*. 4:e5678. http://dx.doi.org/10.1371/journal.pone.0005678

Yuste, R., and T. Bonhoeffer. 2004. Genesis of dendritic spines: insights from ultrastructural and imaging studies. *Nat. Rev. Neurosci.* 5:24–34. http://dx.doi.org/10.1038/nrn1300